Offline commissioning of the multi-reflection time-of-flight mass separator at JYFLTRAP

Master's thesis, 16.12.2019

Author:

Ville Virtanen

Supervisor:

Tommi Eronen

UNIVERSITY OF JYVÄSKYLÄ
DEPARTMENT OF PHYSICS

Abstract

Virtanen, Ville
Offline commissioning of the multi-reflection time-of-flight mass separator at JYFLTRAP
Master's thesis
Department of Physics, University of Jyväskylä, 2019, 36 pages.

In this work, the results from the offline characterisation of the JYFL Multi-reflection time-of-flight mass separator (MR-ToF-ms) constructed at the IGISOL-facility are presented. The separator was used to trap and separate ion bunches consisting of ^{87}Rb and ^{85}Rb. Mass resolving power of $2.6 \cdot 10^4$ was achieved in 2.6 ms in this test. During the characterisation, the use mass-selective ion ejection from the MR-ToF-ms was also tested and found viable.

Keywords:Multi-reflection, time-of-flight, mass, separator

Tiivistelmä

Virtanen, Ville
Moniheijastavan lentoaikamassaspektrometrin käyttöönotto ja karakterisointi stabiileilla ioneilla
Pro gradu -tutkielma
Fysiikan laitos, Jyväskylän yliopisto, 2019, 36 sivua

Tässä työssä esitellään Jyväskylän yliopiston kiihdytinlaboratoriossa sijaitsevaan IGISOL-laitokseen rakennetun moniheijastavan lentoaika-massaerottajan (engl. Multi-Reflection Time-of-Flight mass separator, MR-ToF-ms) käyttöönottokokeen tulokset. Massaerottaja koekäytettiin loukuttamalla ja erottamalla toisistaan samaan ionikimppuun sekoitetut ^{87}Rb ja ^{85}Rb-ionit. Tässä kokeessa laitteella saavutettiin $2.6 \cdot 10^4$ massaerotussuhdeluku 2.6 millisekunnin ajassa. Työssä kokeiltiin myös ionien massavalikoivaa lähetystä moniheijastavasta lentoaika-massaerottajasta jännitepulssitettavan keskuselektrodin avulla onnistuneesti.

Avainsanat: Moniheijastava, lentoaika-massaerottaja, massaspektrometri

Contents

1 Introduction

Mass is one of the fundamental physical quantities to describe an atomic nucleus, as the precise value of an atomic mass is linked to the binding of nucleons to the nucleus via the strong interaction. The main contribution to atomic mass comes from the mass of individual nucleons, that is, the protons and neutrons that are bound to the nucleus. The next significant term is the total binding energy. The binding energy reduces the mass of a nucleus according to the mass-energy equivalence $E = mc^2$. The reduction in energy (or mass) is sometimes called the mass deficit. The total binding energy is the result of various interactions that happen in the nucleus and in the atomic orbitals of electrons, and thus is unique for each type of nucleus. The nuclear binding energy is on the order of MeV per nucleon, whereas the contribution from the binding energies of the electrons to atomic states is orders of magnitude smaller, ranging from few eV to hundreds of thousands of eV per electron. Overall, bound nuclei are about 0.8% lighter than the individual constituents.

The relation between binding energy and atomic mass can be seen in Eq. (1), where the atomic mass $m(A,Z)$ of an isotope that consists of Z protons and N neutrons can be broken down to the contributions from proton and neutron masses m_p, m_n, the mass of an electron m_e and the binding energy $B = B_{\mathrm{nuc}} + B_{\mathrm{e}}$ of nucleons and electrons according to

$$m(A,Z) = Zm_p + (A - Z)m_n + Zm_e - \left(B_{\mathrm{nuc}} + B_{\mathrm{e}}\right)/c^2, \tag{1}$$

where the nuclear binding energy is denoted B_{nuc}, and the atomic binding energy of electrons is denoted B_{e}.

Through the energy-mass equivalence, atomic masses can be directly used to deduce the amount of energy released or needed in a nuclear reaction or decay. For instance, in a reaction of particles denoted by $0 + 1 \rightarrow 2 + 3$ the energy release, which is also called the Q-value is defined as

$$Q_{0+1\rightarrow 2+3} = (m_0 + m_1 - m_2 - m_3) \cdot c^2, \tag{2}$$

where m_i are masses and c is the speed of light. A reaction with a positive Q-value,

releases energy Q, whereas for a negative Q-value the reaction will require at least energy Q for it to be able to happen.

Masses play a significant role in predicting nuclear reaction rates and conditions in stars and other astrophysical environments where the nucleosynthesis of elements takes place through reaction pathways such as the rapid neutron capture process [1].

The nuclear mass also reveals information about nuclear structure. For instance, the two-neutron separation energy, S_{2n}, *i.e.* the binding energy difference of two isotopes with two-neutron difference

$$S_{2n} = B(A,Z) - B(A-2,Z) \tag{3}$$

is sensitive to filling of neutron shells, but insensitive to odd-even staggering, thus giving a useful metric for probing changes in for instance the shape of the nucleus [2]; the filling of nuclear shells can be seen as a distinct drop in S_{2n} at shell closures. The two-neutron separation energies can be used along with other methods for example with the measurement of the mean-square charge radius $\langle r^2 \rangle$ with laser spectroscopy [3] or the measurement of $E(2^+)$ with the means of gamma-ray spectroscopy [4], for identification and extensive study of the nuclear structure.

Several mass models that predict nuclear mass values exist, see for instance references [5]–[8]. While the models predict similar values for masses near stability, the complexity involved in modelling nuclear structure makes the nuclear mass particularly difficult to be accurately reproduced for exotic nuclei, there the models tend to quickly start diverging from each other [9]. In order to both rigorously test these models and to provide more data to work with, it is necessary to develop and utilise experimental techniques that will be able to push measurements further away from the valley of stability and measure the masses of these increasingly exotic nuclei, and at the same time to be able to do so faster and more accurately. The need to measure faster arises from the rapid decrease of half-lives when one moves towards more exotic nuclei.

Experimental methods for determining the atomic mass are available in multitude, and some techniques yield higher accuracy than others. This ability of a mass spectrometer to distinguish ions of differing masses is characterised by it's mass resolving power R,

$$R = \frac{m}{\Delta m}, \tag{4}$$

where m is mass, and Δm is the detectable difference in masses. Another measure of

interest for a method is the accuracy of the mass measurement. Currently, the most accurate atomic mass measurements have been done with Penning traps reaching fractional accuracy of 7 parts per trillion (ppt) in mass ratio with the pulse-and-phase technique [10]. For most techniques, the mass resolving power or accuracy increases with observation time and is therefore limited by the half-life of the ions of interest.

1.1 Motivation

The motivation for this work arose from the need to find a method for mass separation and measurement that was faster than the existing JYFLTRAP Penning trap setup [11] at the IGISOL-facility [12]; the ability to work with increasingly exotic nuclei requires that the needed manipulation and measurement of the ions can be performed before too high a proportion of the exotic ions decay and are lost. A Multi-Reflection Time-of-Flight mass separator (MR-ToF-ms) [13] can reach an order-of-magnitude faster (but not as accurate) mass measurements when compared to the Penning trap, and therefore enables mass measurements of more exotic and short-lived nuclei [13]. For cases where the ions of interest are long-lived enough, the MR-ToF-ms can be used as a fast mass-filter for the Penning trap, allowing for high-accuracy measurements to be made utilising the quickness of the MR-ToF-ms in purification and the accuracy of the Penning trap in measurement. For this purpose, an MR-ToF-ms has been designed and built at the IGISOL-facility. In this work the needed electronics were set up for the MR-ToF-ms and the device was commissioned and characterized using an offline setup.

1.2 IGISOL-facility

The ion-guide isotope-separator on-line facility (figure 1) in the Accelerator Laboratory of the University of Jyväskylä utilizes the IGISOL method [14] developed in Jyväskylä in 1980's, to produce exotic radioactive ion beams. These ion beams are typically used for the study of nuclear structure, nuclear astrophysics, neutrino physics and fundamental interactions (see [15] and the references therein). IGISOL method has several advantages in exploring the nuclear chart when compared to, for instance ISOL-type facilities: both the method's chemical insensitivity [14] and fast ion extraction time of $\leq$ 10–100 ms (depending on the ion guide type) make it possible to produce a wide range of exotic nuclei for studies.

The ions of interest are produced in IGISOL system [14] by directing a high-energy ion beam from the accelerator to the reaction target. The reaction products that are formed in the target are scattered out of the material, losing energy on their way due to straggling, before finally stopping in helium-gas. The products will go through charge-exchange with the helium-gas and thermalize, ending up ionized mostly with charge-state of 1+. The reaction products are extracted from the gas cell to the beam-line with an acceleration voltage of 30 kV. A dipole-magnet is used for coarse mass separation of the reaction products ($R \approx 400$). This is enough to select the mass number (N+Z = constant).

After mass separation, the reaction products are directed to a radiofrequency cooler-buncher [16] where the ions are stopped, cooled, and released in bunches. The ion bunches are then directed either to the collinear laser-line or to the JYFLTRAP purification Penning-trap for finer mass separation. The JYFLTRAP Penning trap [11] is used for high-precision mass measurements, and as a high-resolution mass separator to provide purified beams for decay-spectroscopy studies. The purification trap can be used to reach mass resolving power $R \approx 10^5$ with the mass-selective buffer gas cooling method [17], which is enough to separate ions of interest from an isobaric chain. The mass separation in the purification Penning trap typically takes some hundreds of milliseconds – the shortest time purified beam has been produced with the JYFLTRAP purification trap has been 71 ms with rather modest mass resolving power [18]. Once the ion sample has been purified, it can be used for mass measurements, for more precise mass separation (such as the separation of isomeric states from ground-states) or for post-trap decay spectroscopy.

In a Penning trap, the mass of the ion of interest is measured by determining the ion's cyclotron resonance frequency ν_c in the trap's magnetic field B

$$\nu_c = \frac{1}{2\pi}\frac{q}{m}B, \tag{5}$$

where q/m is the ion's charge-to-mass ratio. The time-of-flight ion-cyclotron resonance (ToF-ICR) technique [19] and the Phase-imaging ion-cyclotron-resonance technique (PI-ICR) [20] are the methods used for mass measurements at JYFLTRAP. The accuracy of measurement increases linearly as a function of the measurement time for a Penning trap.

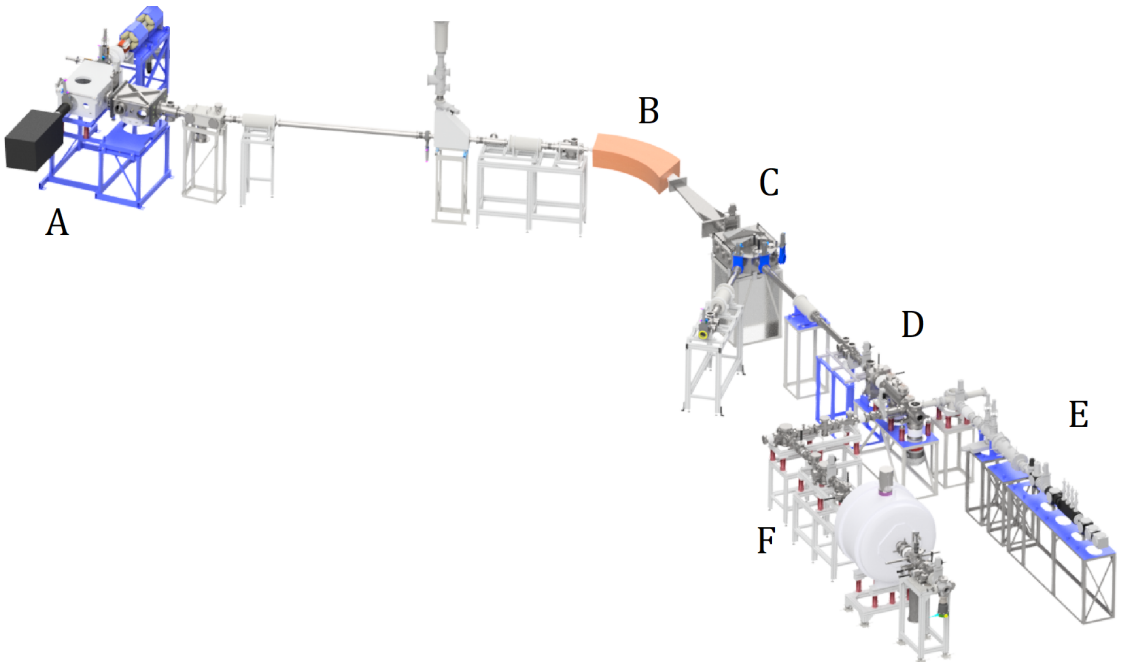

Figure 1. The IGISOL facility. (A) IGISOL target area, (B) dipole magnet, (C) switchyard, (D) radiofrequency cooler-buncher, (E) collinear laser line, (F) JYFLTRAP double Penning trap.

1.3 A needle in a haystack

A common challenge in studying short-lived exotic nuclei produced in radioactive ion-beam facilities is the removal of the vast background of uninteresting nuclei from the sample. Production yields for contaminants can be orders of magnitude more than for the nuclei of interest. figure 2 shows the detected number of ions versus the ion mass measured using purification Penning trap of JYFLTRAP. The ions were produced in 25-MeV proton induced fission reaction with natural uranium. Evidently, ^{115}Ru is significantly less produced than the other isobars ^{115}Rh, ^{115}Pd, ^{115}Ag and ^{115}Cd.

In addition to the contamination originating from nuclear reactions, there can be contamination originating from impurities in the buffer gas. Removal of the contaminants takes time, and sometimes limits the amount of ions that can be measured, for example due to space charge limits in a Penning trap. To alleviate this issue, a multi-reflection time-of-flight mass separator is being installed to complement the Penning trap. This allows purification of larger quantities of ions in shorter time

[13]. Additionally, faster measurement cycle helps to minimize decay losses due to radioactive decay.

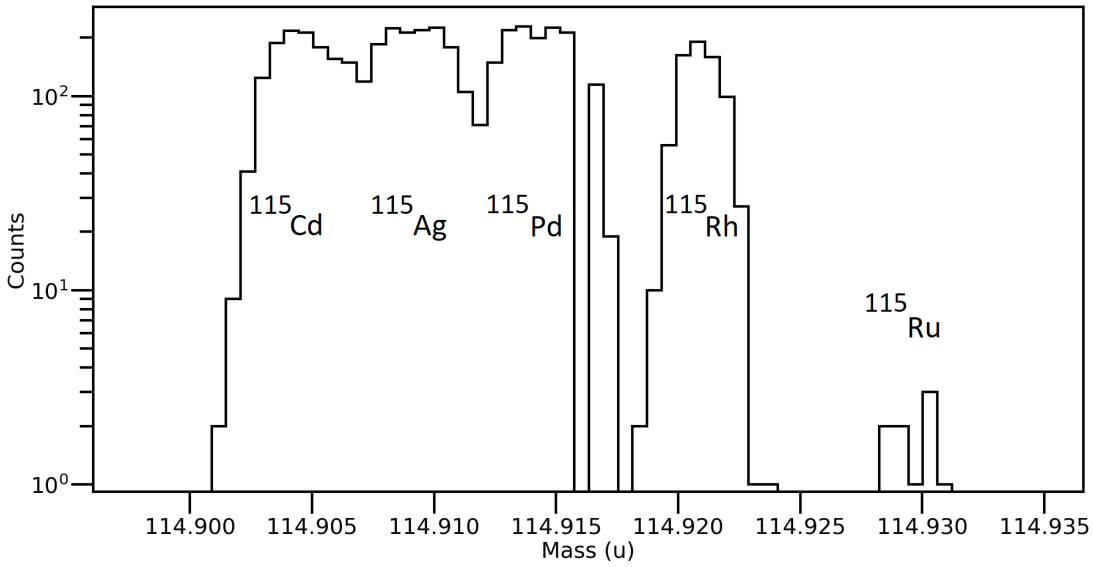

Figure 2. Mass scan in the purification Penning trap. Due to lower production rate and shorter lifetime, the more exotic (and thus heavier) ^{115}Ru ions are significantly less produced than ^{115}Rh, ^{115}Pd, ^{115}Ag, and ^{115}Cd. Highest peaks likely suffer from saturation effects of the ion counter.

2 Multi-reflection time-of-flight mass separators

The operation principle of an MR-ToF-ms [13] is based on temporally separating ions by their mass by trapping and reflecting them in an energy-isochronous potential between two electrostatic mirrors. In this potential, the time-of-flight t of individual ions does not depend on the ion's kinetic energy E. The time-of-flight is then proportional to ion mass-to-charge ratio $t \propto \sqrt{m/q}$. The separator's mass resolving power R can then be estimated with $m \propto A \cdot t^2$ and $\mathrm{d}m \propto 2A \cdot t \cdot \mathrm{d}t$ to find

$$R = \frac{m}{\Delta m} \approx \frac{A \cdot t}{2A \cdot \mathrm{d}t} \approx \frac{t}{2\Delta t}, \tag{6}$$

where Δt is the full width at half-maximum of time-of-flight distribution.

Time-of-flight between points x_1 to x_2 can be found generally for a positively charged particle in some potential $U(x)$ by

$$t(E) = \sqrt{\frac{m}{2}} \int_{x_1}^{x_2} \frac{dx}{\sqrt{E - qU(x)}}. \tag{7}$$

The simplest (single-pass) time-of-flight separator is to let the ion bunch fly a fixed distance $d = x_2 - x_1$ in constant (ground) potential, where the time of flight of an ion will be

$$t(E) = \sqrt{\frac{m}{2}} \frac{d}{\sqrt{E}}. \tag{8}$$

As equation (8) implies, the achievable time-of-flight difference between different masses is restricted by the drift length d. By trapping the ions in a potential where they move multiple turns in closed paths, the drift length d is significantly increased. This increases the mass resolving power, provided that the bunch widths do not get increasingly wider as the bunch cycles in the device.

The drift potential between the MR-ToF-ms and the ion detector is not energy-isochronous and thus the MR-ToF-ms has to be tuned carefully to create a time-focus (that is, a minimum in time-of-flight distribution width) at the detector plane. When the length of the flight-paths extends, small aberrations in the MR-ToF-ms potential caused by, for instance, imperfect mirrors and fluctuations in mirror electrode voltages affect the ion time-of-flight and makes it possible for differences in ion initial energy

to cause differences in ion time-of-flight. The ion bunch initially has energy spread that originates from the extraction from the ion buncher. This spread makes the resolving of the different mass peaks from each other more difficult.

In reality, an MR-ToF-ms is not perfectly energy-isochronous and the time evolution of the temporal bunchwidth needs to be estimated and tuned with mirror voltages in order to optimise the mass-resolving power. In addition to the flight between the MR-ToF-ms and the detector, the flight between the ion source and the MR-ToF-ms is not energy-isochronous. To maximize R, these effects need be taken into account in order to have the time focus plane at the ion detector. In practice, the time-focus is adjusted by changing the device's time-of-flight—energy dispersion coefficient $\partial\delta_{\mathrm{T}}/\partial\delta_{\mathrm{E}}(E)$, which can be done by changing the ions' mean kinetic energy with, for example, the in-trap lift [21].

One can estimate the mass resolving power of a realistic, time-focus matching device by

$$R \cong \frac{t_{\mathrm{transfer}} + nT}{2\sqrt{\Delta t_{\mathrm{th}}^2 + \left(\Delta t_{\mathrm{E}} - nT\left(\frac{\partial\delta_{\mathrm{T}}}{\partial\delta_{\mathrm{E}}}\right)\Delta\delta_{\mathrm{E}}\right)^2 + \left(\Delta t_{\mathrm{A}} + n\Delta T_{\mathrm{A}}\right)^2}}, \tag{9}$$

where n is the number of revolutions in the MR-ToF-ms, t_{transfer} is the total time-of-flight during which the ions are not considered trapped. In order to estimate the total time width of the ion bunch, the lower limit for time-of-flight spread Δt_{th}, defined by thermal distribution of ions originating from the ion source needs to be taken into account. Δt_{E} is the ion bunch time spread accumulated before the ions enter and after the ions leave the device. One can also estimate the amount the time spread evolves during the time that the ions are trapped in the MR-ToF-ms by finding the ions' relative kinetic energy spread $\Delta\delta_E$ and the time-of-flight energy dispersion coefficient $\partial\delta_{\mathrm{T}}/\partial\delta_{\mathrm{E}}$. Aberrations to the time-of-flight spread are contained in the terms Δt_{A} and $\Delta T_{\mathbf{A}}$ [22]. For a more detailed explanation of the terms of the mass resolving power equation, see references [21] and [22].

2.1 JYFL MR-ToF-ms

The electric potential of an MR-ToF-ms is defined by the geometry and voltages of the mirror electrodes. In the JYFL device (figure 3), there are six pairs of cylindrically symmetric mirror electrodes, placed symmetrically around the in-trap lift electrode [21], a pulsed drift-tube that is used to change the ions potential energy in order to trap them for separation. An example of the JYFL MR-ToF-ms potential simulated with SIMION can be seen in figure 4. SIMION uses both Runge-Kutta and finite difference methods to solve partial and ordinary differential equations to deduce particle trajectories [23]. A simplified trapping and separation procedure with the JYFL MR-ToF-ms is illustrated in figure 5.

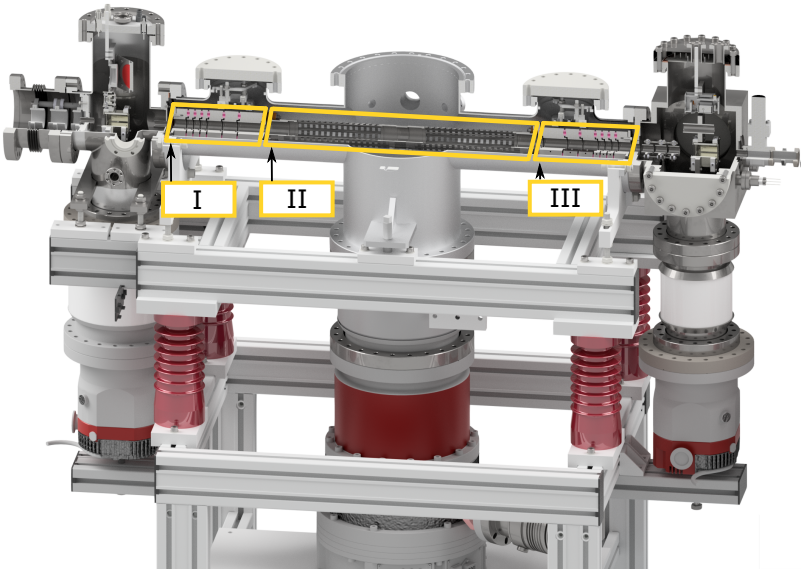

Figure 3. JYFL MR-ToF-ms. Six pairs of mirror electrodes (I and III) and a pulsed drift tube (II) define the potential the ions trapped in the mass separator experience.

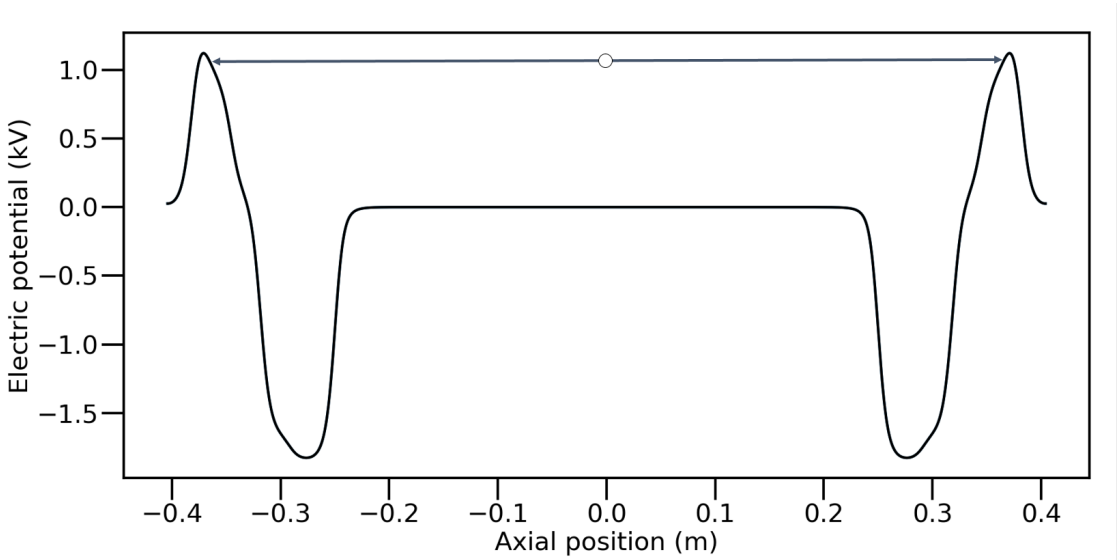

Figure 4. Simulated electric potential along the axis of symmetry in the JYFL MR-ToF-ms. This potential is tuned for ions with 1 keV of kinetic energy.

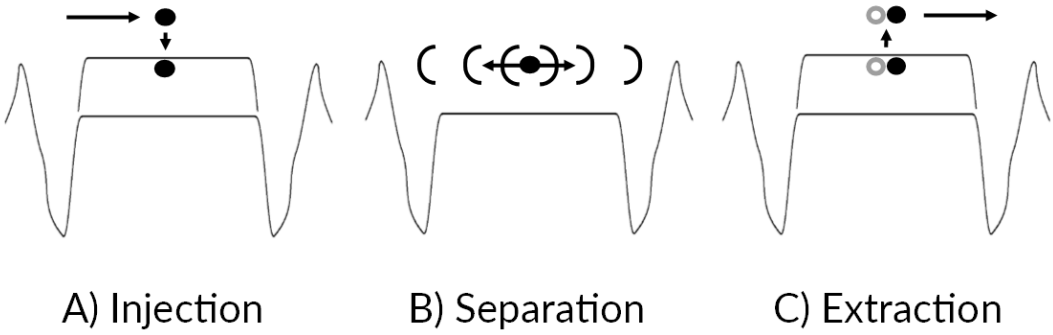

Figure 5. Principle of ion injection, mass separation and ion extraction using the pulsed drift tube. (A) The ions are injected with enough energy to pass the mirror potential. While the ions are in the drift tube, the voltage of the tube is pulsed down to reduce the ion's potential energy. (B) The ions no longer have enough energy to pass the mirror potential, and are reflected along closed paths in the device. (C) Once different masses have accumulated enough time-of-flight difference to be resolved, the in-trap lift is used to increase the potential energy of the ions so that the ions are able to leave the device.

2.2 Voltage stabilization circuit

The electrostatic potential wherein the ions are cycled is defined by electric potentials of individual mirror electrodes. For this reason, the stability of a voltage supply limits the mass resolving power as temporal fluctuations widen the peaks in a time-of-flight distribution. To further study this, the sensitivity of ion time-of-flight to changes in individual mirror voltages was simulated with SIMION, see figure 6. By far, the fifth mirror electrode is the most sensitive to fluctuations in the typical potential configuration. This is because the fifth mirror electrode is close to the ion's reflection point and so the ions spend more time close to this electrode.

It was concluded that to achieve good long-term voltage stability, a PI-circuit (proportional-integral, figure 7) similar to that in use at ISOLTRAP at CERN [24] should be implemented to stabilize the voltage of mirror electrode 5. Such a circuit consists of a low-pass filter, which attenuates any short time-scale voltage fluctuations, and a PI-loop which handles the long time-stability of the voltages. Since the voltages used in the mirrors are relatively high (~ 1 kV) for the multimeter, an Ohm-labs KV-10A voltage divider was also used. The PI-loop was set to adjust the voltages every 80 ms. Although the PI-loop itself could react faster if needed, the used ISEG-EHS 8240X voltage-supply cannot update voltage set-values faster than every 80 ms and so the voltage supply is the limiting factor in the responsiveness of the circuit.

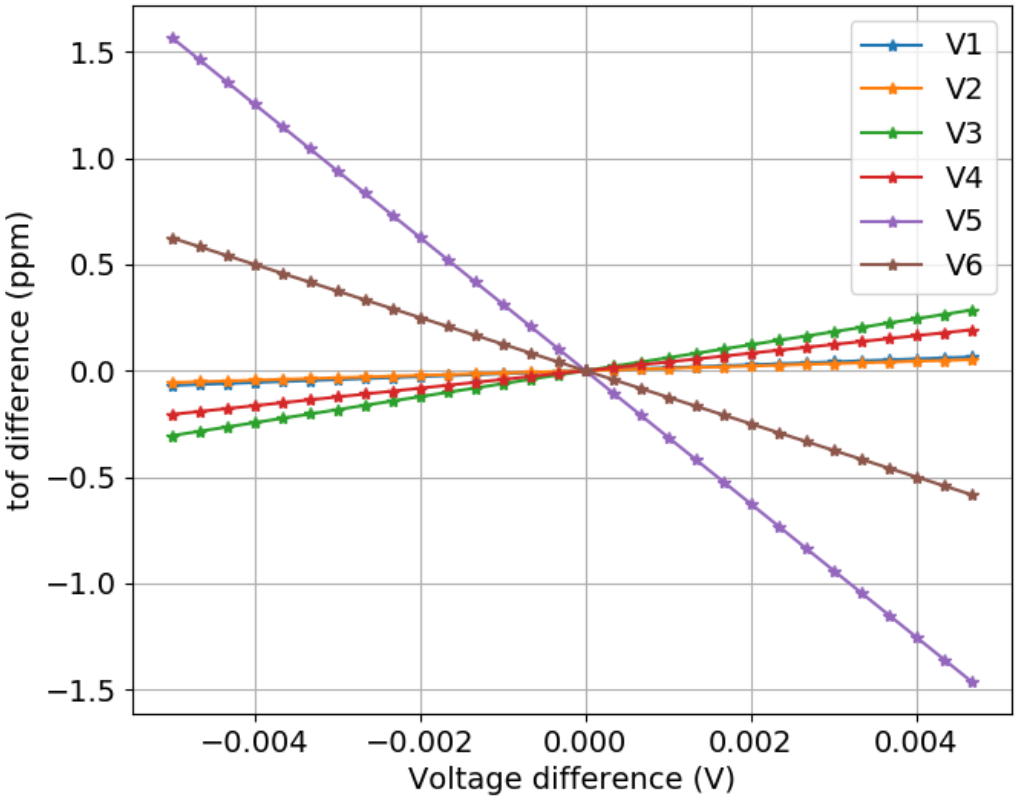

Figure 6. Simulated ion time-of-flight difference per round as a function of the mirror electrode voltage difference in the MR-ToF-ms. Mirror electrode 1 is closest to the drift tube, and 6 is the furthest from it. Simulations were carried out with SIMION. Mirrors 5 and 6 (the two furthest away from the drift electrode) are the most sensitive to voltage changes.

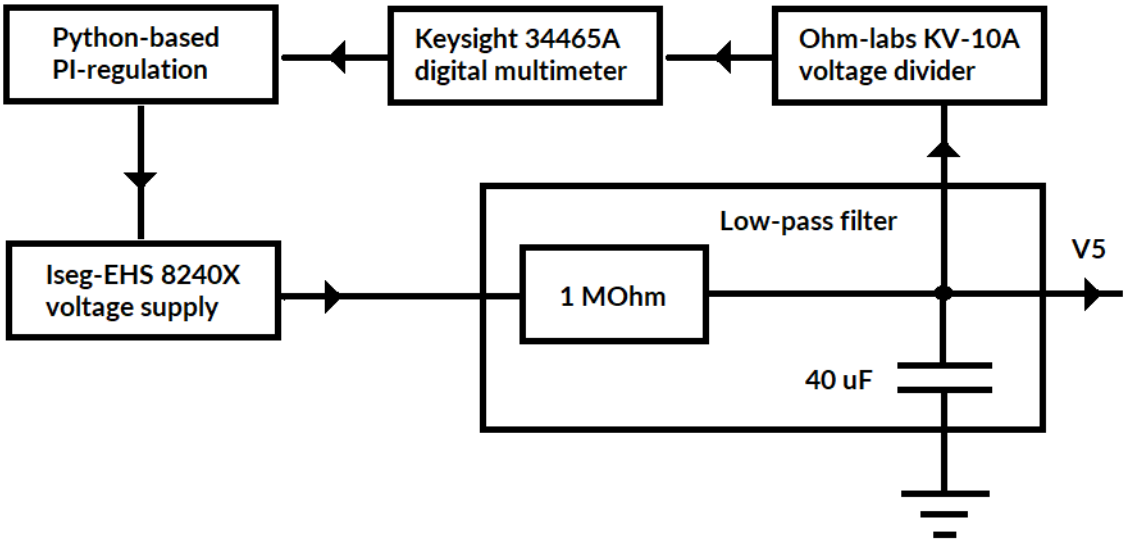

Figure 7. Stabilization circuit scheme. The circuit consists of a voltage supply, a low-pass filter, a voltage divider, a digital multimeter and a computer that runs the PI-loop.

3 The test setup

To perform offline characterisation for the MR-ToF-ms, an offline test-setup (figure 8) was assembled. For this test, a surface ion-source containing naturally abundant potassium (^{39}K, ^{41}K), rubidium (^{85}Rb, ^{87}Rb) and caesium (^{133}Cs) was used. As the work function for these elements is very low, singly charged ions were produced by just heating the source. The singly charged ions were accelerated to 2 keV of kinetic energy. The continuous beam was then directed through a Bradbury-Nielsen ion gate [25], [26], which was used to chop the beam into bunches by pulsing the voltages on the gate grid wires off for 150 ns every measurement cycle. To ensure parallel and centred bunches, the bunched beam was then collimated with two collimators having diameter of 1.7 mm and distance of 40 mm. The collimators also served as a differential pumping barrier between the MR-ToF-ms and the bunch preparation-stage.

The MR-ToF-ms should have as good vacuum as possible to minimize ion losses from collisions with any background molecules. During the tests the MR-ToF-ms had $\sim 2 \cdot 10^{-9}$ mbar vacuum, as measured from the drift-tube chamber. The mirror electrode voltages were supplied with ISEG-EHS 8240X multi channel voltage-supplies and remotely controlled with a control program written in python. The in-trap lift voltage was supplied through a high-voltage switch (BEHLKE HTS-61-03-GSM), with rise-time of 100 ns. The switch timing was controlled using a timing card (Spincore Pulseblaster PB24-100-24k-PCI). The ions were trapped by setting the in-trap lift voltage to +1 kV so that the ions slowed down to 1 keV after entering the in-trap lift electrode. Once the ions are in the trap, the voltage was switched to ground potential to trap the ions inside the device. After cycling the ions in the MR-ToF-ms, they were ejected to a MagneToF ion detector [27], [26] from which the output signal was passed to a Fast Comtec MCS6A [28] time-to-digital converter (TDC), and finally recorded with the MPANT-program [29]. The MagneToF-detector and the TDC combined have great time resolution; the detector pulse width is $\sim$ 400 ps [27] and the TDC's pulse width resolution is 256 ps [28]. The voltages that were used in this work are presented in table 1.

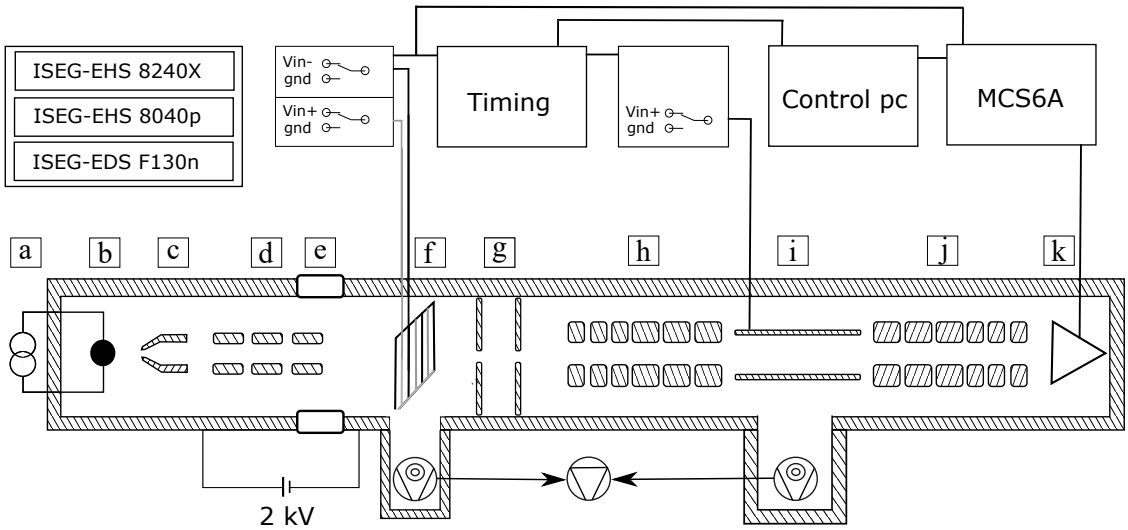

Figure 8. MR-ToF-ms offline characterization set-up. (a) Heating current for the surface ion-source (b). (c) skimmer-electrode, (d) an einzel-lens, (e) a plastic insulator, (f) Bradbury-Nielsen gate, (g) a set of two 1.7 mm diameter annular collimators, doubling as a differential pumping barrier, (h) injection-side mirror electrodes, (i) in-trap lift pulsed drift-tube, (j) extraction-side mirror electrodes, (k) a MagneToF detector. The setup was kept in vacuum with two turbomolecular pumps that were connected to a scroll pump. The voltages for the sensitive mirror electrodes were supplied with the ISEG-EHS 8240X, whereas the voltages for the Bradbury-Nielsen gate voltage switches, in-trap lift voltage switch, the 2 kV ion acceleration voltage and the bias for the MagneToF detector were supplied with the ISEG-EHS 8040p and ISEG-EDS F130n modules. The control pc was used to control the timings, to control the voltages, and the MPANT-program to record the ToF-data.

Table 1. MR-ToF-ms offline test voltages. All the mirror element voltages were supplied with the high-stability and high-precision 4-kV ISEG-EHS 8240X-module. The rest of the positive voltages were supplied with the ISEG-EHS 8040p (max +4 kV), and the other negative voltages were supplied with the ISEG-EDS F130n (max -3 kV).

Element	Voltage [V]
Acceleration	2000.0
Skimmer	1930.0
Einzel-lens	1032.0
Bradbury-Nielsen gate	±250.0
Mirror electrode 1	-1841.9
Mirror electrode 2	-1659.6
Mirror electrode 3	100.0
Mirror electrode 4	904.7
Mirror electrode 5	1008.7
Mirror electrode 6	1468.2
In-trap lift electrode	1006.0
Bias for MagneToF	-2640.0

4 Results

In the first test, the stability of the voltage source and the stabilization circuit was studied. In the rest of the tests, an offline ion-source containing ^{39}K, ^{41}K, ^{85}Rb, ^{87}Rb and ^{133}Cs was used to create ion bunches, by chopping the initially continuous 2 keV beam to 150 ns wide bunches with a Bradbury-Nielsen gate. The chopped beam was then directed through a 1.7 mm diameter annular collimator to have a beam that was both parallel to the MR-ToF-ms's optical axis and centred to it.

4.1 Stability

To test the stability of the mirror voltages supplied by ISEG-EHS 8240X, the voltage of mirror electrode 5 was logged with a Keysight 34465A-digital multimeter for three cases: baseline voltage from the source with no modifications, voltage with a low-pass filter and low-pass filter with PI-regulation (figure 7). Allan deviations [30] of these datasets are presented in figure 9. The PI-regulation was able to reduce long time-scale ($\tau \sim 800$s) voltage Allan deviation from 1.27 ppm (parts per million) to 0.0136 ppm, however, the short-term ($\tau \approx 1$ s) deviation increased from 0.8 ppm to 2 ppm — a significant increase — and falls below the baseline at $\tau = 11$ s. It looks like the circuit is overshooting the short time-scale corrections, but manages to stabilize the voltages over long timescales. If indeed the jump is due to overshooting, it should be possible to fix it by finetuning the PI-parameters. It is also worth noting that although the low-pass filter reduces the Allan deviation for most of the measurement range, at $\tau \sim 1$ s the deviation increases slightly. The difference, however, is less than 0.3 ppm of mirror voltage, and not significant.

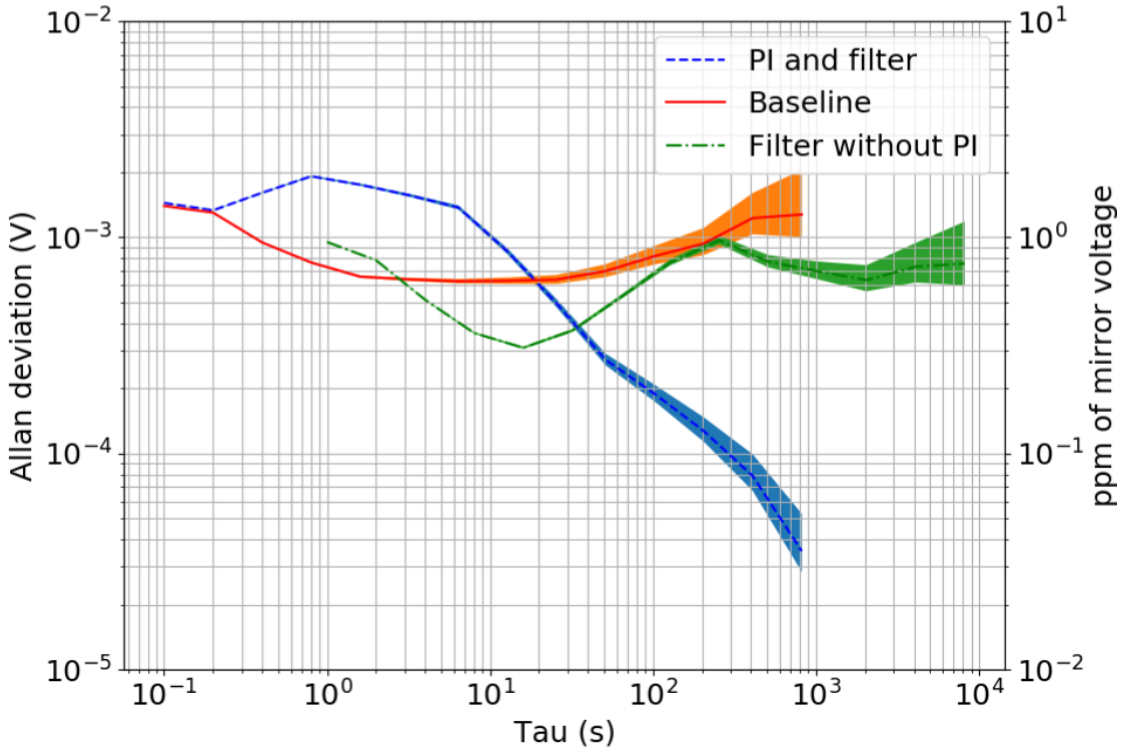

Figure 9. Allan deviation in voltage of the electrode 5. The mirror voltage was set to 1 kV. The curves for baseline and PI show the PI-loop reducing the long-term Allan deviation by a factor of nearly two orders of magnitude, when compared to the unmodified system. Clearly, the circuit needs to be tuned better to reduce the deviations at $\tau < 20$ s.

4.2 Trapping and mass separation

In the first test with ions, a bunch containing ^{87}Rb and ^{85}Rb ions was trapped and stored until the isotopes of rubidium were separated. To get a better idea of the time-of-flight separation of masses that happens without trapping, a reference time-of-flight spectrum for bunches that have flown straight through the test-setup is shown in figure 10. A simple shoot-through is enough to separate K, Rb and Cs from each other due to their large differences in atomic mass. Still, isotopes closer in mass, such as ^{87}Rb and ^{85}Rb, remain unresolved from each other. When ^{87}Rb and ^{85}Rb are trapped and stored for 12 rounds of flight in the MR-ToF-ms, they are

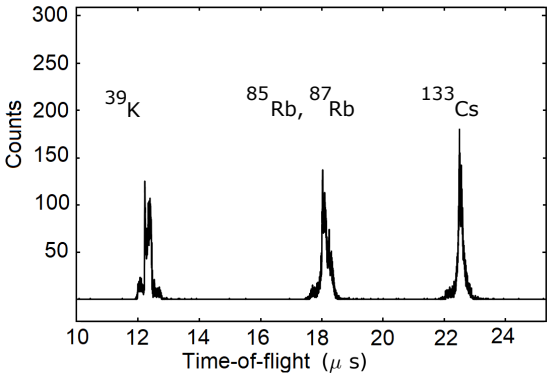

Figure 10. Reference time-of-flight spectrum from offline ion-source with the MR-ToF-ms using shoot through mode.

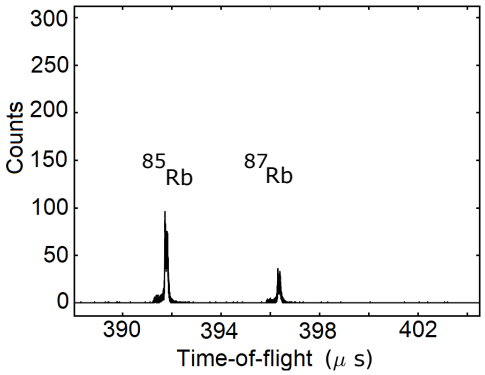

Figure 11. Time-of-flight spectrum of ^{85}Rb and ^{87}Rb after 12 rounds of flight in the MR-ToF-ms.

clearly resolved from each other in less than 0.4 ms, see figure 11.

4.3 In-trap lift voltage and ion time-of-flight

To study the effect of ion kinetic energy on the ion time-of-flight in the MR-ToF-ms, the in trap-lift voltage was scanned while keeping the mirror voltages unchanged. The voltage scan was performed for ^{133}Cs ions that were trapped and cycled for 500 revolutions in the MR-ToF-ms. The scan results have been plotted in figure 12. The smallest energy-dependence for time of flight can be found between 1000 and 1020 V (corresponds to ion kinetic energies of 1000 eV and 980 eV), where the time-focus plane has been adjusted to be close to the detector. For some reason, majority of the ions are lost between in-trap lift voltages of 950 and 930 V. One possible reason for this could be that the change in ion kinetic energy had affected the ion period of oscillation so much that the ions were not inside the in-trap lift electrode, and thus not extracted for this reason. It is clear from the scan that the ion transmission depends on ion kinetic energy, as slices from the main plot taken at 940V and 994V show.

As equation (9) implies, both the bunch mean time-of-flight and the time evolution of bunchwidth in the scan are affected by the ion mean kinetic energy. Perhaps counter-intuitively, around different voltages small changes in kinetic energy affect ion time of flight differently. For instance, between 950V and 970 V, the decrease of kinetic energy leads to a longer time-of-flight, but between 980V and 990V the

opposite is true. Changes in ion kinetic energy seem to have the smallest impact around 1010 V. From this scan it is clear, that to maximize the mass resolving power, the in-trap lift voltage needs to be tuned carefully and it also needs to be stable.

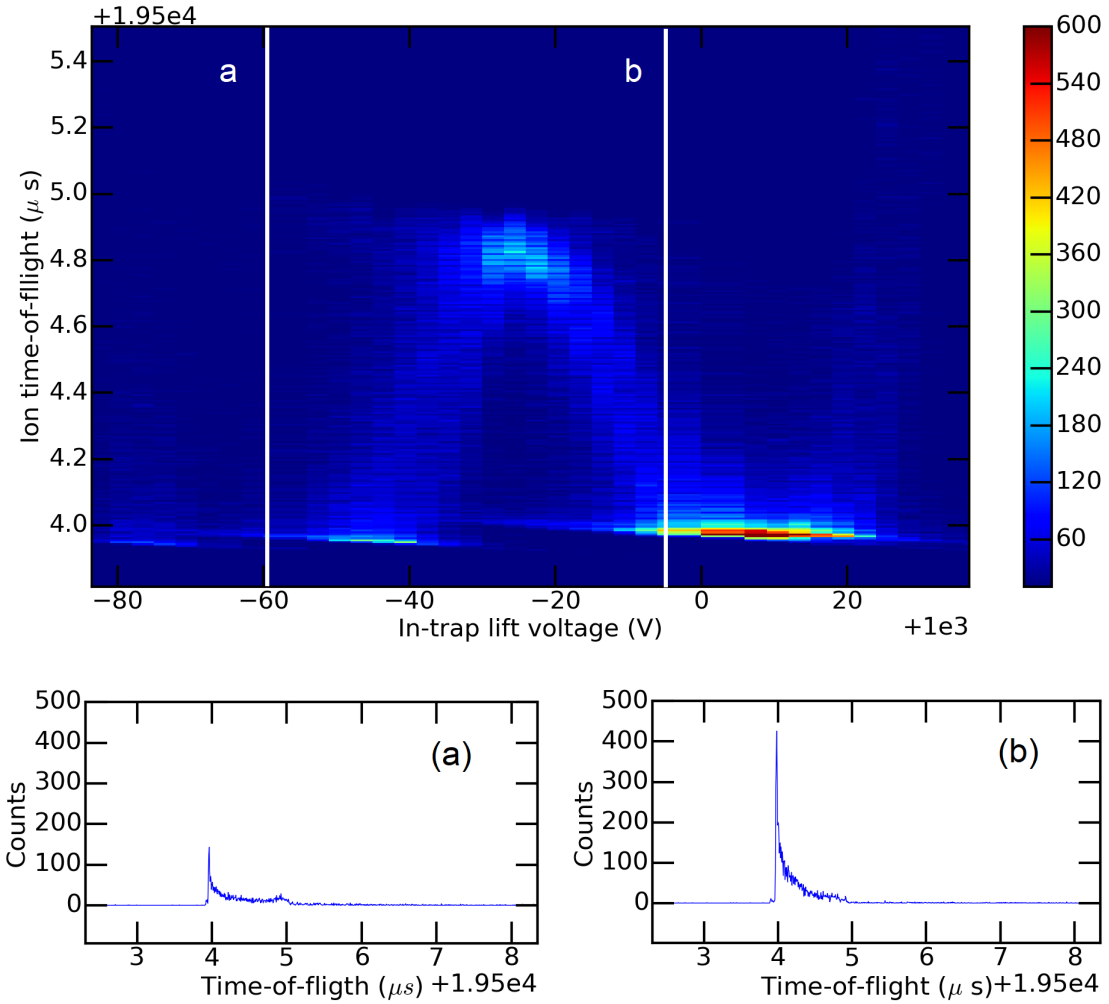

Figure 12. Counts and time-of-flight of bunched ^{133}Cs as a function of the in-trap-lift pulsing voltage for 500 rounds of flight in the MR-ToF-ms. Plot (a) is obtained with in-trap lift voltage of 940 V and (b) with 994 V.

4.4 Mass selection with the in-trap lift

To study the possibility of using the in-trap lift for mass-selective ion ejection [22] with the JYFL MR-ToF-ms, ^{85}Rb, ^{87}Rb and ^{133}Cs were trapped and cycled in the MR-ToF-ms for 2.6 ms. For this test, unfortunately, the different ions are too easy to separate. Therefore the timing was selected so as to simulate a more realistic case with isobaric masses *i.e.* a case where the three bunches of different masses were temporally separated, but close to each other. First, a simple in-trap lift timing pattern was used (figure 13). Using this pattern, the timing of pulsing the drift tube to higher electric potential after trapping and cycling was scanned over 16 μs to produce figure 15. By changing the time of pulsing the in-trap lift electrode voltage, different limits for extracted masses can be set by their time-of-flight. The subplots of figure 15 show varying selections of masses, but as can be seen from the subplots of this figure, one can only set an upper or lower limit on the time-of-flight in this way. This pattern is not enough to select a single mass, unless that mass is the first or the last in the time-of-flight spectrum. However, by setting both upper and lower limit for the time-of-flight with early and late switching [22] (see figure 14), any single mass can be selected, provided that it is sufficiently well-resolved from its neighbours.

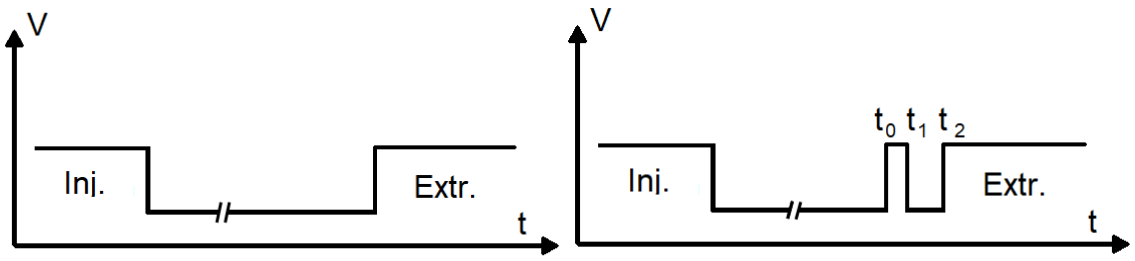

Figure 13. Voltage timing pattern for bunch injection, storage and extraction with the in-trap lift. Typically in-trap lift voltage is switched when the ions of interest are halfway through the drift-tube. However, by placing the ions of interest just inside the drift tube, while leaving other ions just outside the lift, one can selectively eject ions based on their time-of-flight, while rejecting ions with less or more time-of-flight – depending on which edge of the drift tube is used. This is realized by moving the edge of the extraction pulse with relation to the trapped ToF-spectrum [22].

Figure 14. Voltage timing pattern for mass selective ToF-gating that uses both late and early switching patterns. Times t_0, t_1, and t_2 are tuned so that all except the ions of interest will be removed. The width of the ToF-gate is dependent on $t_2 - t_1$.

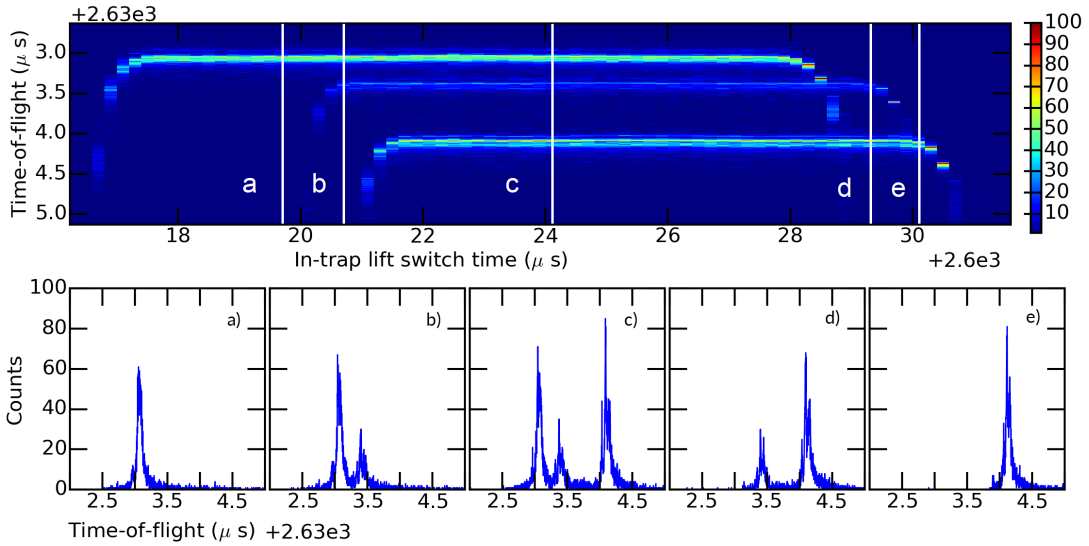

Figure 15. ^{85}Rb , ^{87}Rb and ^{133}Cs time-of-flight as a function of the in-trap lift switch time at around 2.6 ms of storage time. Subfigures (a)-(e) correspond to timings marked by vertical lines in the top-part of the figure. With timing (a) and (e), only one ion species is able to exit the device, with (b), (c) and (d) two or all are able to exit. As long as the ions are inside the in-trap lift electrode when the voltage is switched, their ToF is constant. In the case of early switching, when the lift's electric potential is switched high slightly before the ions are in the lift, ions don't gain potential energy. In the case of the late switching, the ions don't gain potential energy. So the ions receive less total kinetic energy on their way out and thus are slower or even not able to exit the device.

The same isotopes ^{85}Rb, ^{87}Rb and ^{133}Cs were used in the next test to demonstrate separation of any mass, whether it is the first, last or in the middle of the ToF-spectrum. The in-trap lift timing scheme can be seen in figure 16. This pattern uses a combination of late and early switching introduced in [22]. In this case, both edges of the in-trap lift are used for ion selection: One edge is used to reject ions with smaller ToF and the other edge to reject ions with longer ToF than the ions-of-interest. By changing timing parameters t_0, t_1 and t_2, the time-of-flight acceptance window can be adjusted. In this case, t_0 was fixed while t_1 was scanned over the spectrum with three fixed window widths (t_2-t_1): 3.1 μs, 2.1 μs and 1.1 μs. The effect of this time-of-flight gate can be seen as the in-trap lift timeband narrows for each mass. At 1.1 μs window width, all the peaks are isolated, and can be individually selected. For

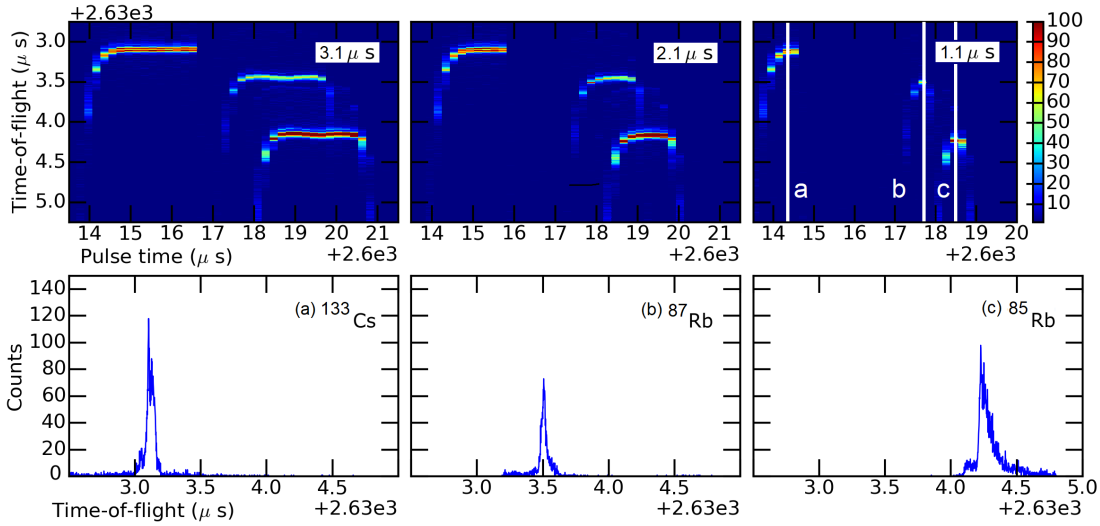

Figure 16. In first row, timing scan for mass-selective ion ejection with 3.1 μs, 2.1 μs and 1.1μs window widths. Lower row: ^{133}Cs, ^{87}Rb and ^{85}Rb selected with timings marked by vertical lines in the top-right subplot.

cases close by each other, the edge field of the in-trap lift will affect the time-of-flight somewhat.

4.5 Mass range and sources of error

To reach best mass precision, it is best to limit the measurement only to ions that are still on the same lap in the separator. There are several reasons for it. For instance, disentangling a ToF-spectrum that consists of mass peaks that have travelled different number of laps requires more complicated analysis, and comes with the risk of introducing shifts to the time-of-flight of ions. This error can be introduced when ions on different laps have not flown over identical potential [31]. Furthermore, ions that are on different laps will not have their time-focus on the same plane.

Requiring that the measured ions exited while still on same lap will limit the mass range that can be measured due to the limited length of the in-trap lift; although the mass resolving power of the MR-ToF-ms increases over the number of revolutions, the range of masses that are still on the same lap and can simultaneously fit inside the in-trap lift electrode decreases over time, as the time-of-flight difference between

masses increases.

Upper and lower limit for the mass resolving power can be estimated. They can be interpreted to correspond to the highest and lowest measurable mass ranges based on two extreme cases of where the resolved masses are still on the same lap and within the in-trap lift electrode. The first case — which corresponds to the highest mass resolving power — is bunches that are only just resolved, that is, two times the full width half maximum of their ToF-peak apart. The lower mass resolving power (or the maximum mass range) limit is found by considering bunches that are separated by the time the ion takes to fly through the in-trap lift, τ_{itl}. These limits can be estimated based on the period of oscillation, the time the ion spends in the field-free region in the in-trap lift (flat part of the bands seen in figure 15) and the bunch width in the MR-ToF-ms, and assuming time focus can be found for each lap, *i.e.* that the bunch width can be kept to the same width as in figure 16.

Using the results for ^{87}Rb, these mass resolving powers are plotted in figure 17 as function of the number of revolution. In figure 17, the area above the full red line can be interpreted as masses that are on the same lap but have not yet been resolved with the current bunch width. The area below the blue dotted line can in turn be interpreted as cases where masses corresponding to the mass resolving power on the y-axis have been resolved so far away from each other, that they no longer fit in the drift tube at the same time. This estimate provides an upper limit for the mass resolving power and mass range. It should be noted, however, that the increase in mass resolving power cannot be sustained indefinitely.

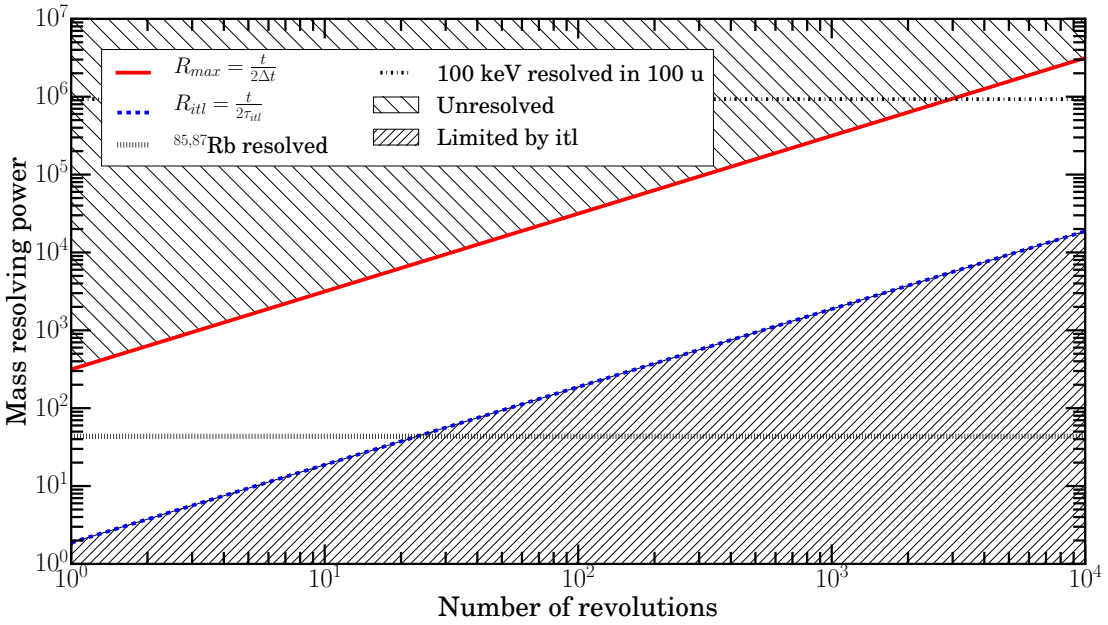

Figure 17. The currently available mass resolving power for given number of revolutions is drawn with solid red line. Anything above the red line are not resolved. The dotted blue line shows the lowest possible mass resolving power, which is also the mass range that simultaneously fits in the in-trap lift. The higher horizontal line marks the mass resolving power (10^6) that is needed to separate 100 keV/c^2 out of mass 100 u. The lower horizontal line marks the mass resolving power (≈ 40) required to separate ^{87}Rb from ^{85}Rb.

As measurement times increase linearly with the number of revolutions, the effects of fluctuations in the mirror potentials, misalignment and other such unwanted effects also increase. In practise, the bunch width cannot be kept constant indefinitely. The mass resolving power will in reality start to saturate for higher number of laps. The area between the red solid line and the blue dotted line therefore represents an upper limit for the range of mass resolving powers that can be achieved for a given number of laps. To get a realistic idea of this saturation through measurement, however, will require using higher current of bunched ions, available from the RFQ cooler-buncher with it's characteristic energy and time distributions, along with a more sophisticated fitting function for the ToF-peak shape, such as the hyper-EMG [32]. This will allow to study effects of bunch energy dispersion and space-charge on the evolution of bunchwidth, time-of-flight and the mass resolving power over long timescales.

5 Discussion

In this work, the JYFL MR-ToF-ms has been used for the first time to trap, separate and isolate ^{85}Rb and ^{87}Rb ions. Mass resolving power of $R \approx 2.6 \cdot 10^4$ was reached with roughly 2.6 ms separation time. Assuming time focus comparable to that achieved in these tests can be retained for a higher revolution numbers (figure 17), at 26 ms the mass resolving power for ^{87}Rb would be $R \approx 2.6 \cdot 10^5$. When compared to the performance of the technically similar MR-ToF-ms at ISOLTRAP, the performances of these devices seem very similar: $R \approx 1.5 \cdot 10^5$ in 25 ms for separation of ^{50}Ti from contamination of ^{50}Cr, or $\sim 2.0 \cdot 10^4$ in 2.6 ms for m = 90 u with the ISOLTRAP MR-ToF-ms [33].

An isobaric ion source (e.g. containing stable ^{115}In and ^{115}Sn) could be used to study more complicated effects on the evolution of the bunchwidth and mass resolving power (such as space-charge, see for instance [34] and the references therein), while keeping the masses on the same revolution number. With this in mind, it would be interesting to further study how the ions' kinetic energy affects the period of revolution of ions and the time focus.

The sensitivity and stability of the MR-ToF-ms has been studied with simulations, and its performance has been tested in use. The PI-based stabilization was able to reduce the long-term voltage fluctuations significantly. The short-term fluctuations, however, need to be studied more carefully.

It is apparent, that in order to reach faster purification times and higher mass resolving power, the bunchwidth and the energy dispersion of the ions of interest need to be sufficiently low for achieving good mass resolving power. It might be necessary to upgrade the cooler-buncher to accommodate the requirements of the MR-ToF-ms.

The mass-selective ion ejection-technique [22] has been studied and implemented with promising results. This eliminates the need for a Bradbury-Nielsen ion gate, and could in future be used to limit effects of space-charge by removing contaminants as soon as they separate from the ions of interest. At the time of the writing of this thesis (12/2019), the MR-ToF-ms has been installed as part of the on-line setup at the IGISOL-facility.

References

[1] A. Cameron, "Stellar evolution, nuclear astrophysics, and nucleogenesis," Atomic Energy of Canada Chalk River Report CLR-41., Tech. Rep., 1957.

[2] D. Lunney, J. M. Pearson, and C. Thibault, "Recent trends in the determination of nuclear masses", *Reviews of Modern Physics*, vol. 75, no. 3, pp. 1021–1082, 2003. DOI: 10.1103/revmodphys.75.1021.

[3] P. Campbell, I. Moore, and M. Pearson, "Laser spectroscopy for nuclear structure physics", *Progress in Particle and Nuclear Physics*, vol. 86, pp. 127–180, 2016. DOI: 10.1016/j.ppnp.2015.09.003.

[4] R. Cakirli and R. Casten, "Nuclear binding and nuclear structure", *International Journal of Mass Spectrometry*, vol. 349-350, pp. 187–191, 2013. DOI: 10.1016/j.ijms.2013.04.011.

[5] J. Duflo and A. Zuker, "Microscopic mass formulas", *Physical Review C*, vol. 52, no. 1, R23–R27, 1995. DOI: 10.1103/physrevc.52.r23.

[6] N. Wang *et al.*, "Surface diffuseness correction in global mass formula", *Physics Letters B*, vol. 734, pp. 215–219, 2014. DOI: 10.1016/j.physletb.2014.05.049.

[7] S. Goriely, N. Chamel, and J. M. Pearson, "Further explorations of skyrme-hartree-fock-bogoliubov mass formulas. XIII. the 2012 atomic mass evaluation and the symmetry coefficient", *Physical Review C*, vol. 88, no. 2, 2013. DOI: 10.1103/physrevc.88.024308.

[8] M. Kortelainen *et al.*, "Nuclear energy density optimization", *Physical Review C*, vol. 82, no. 2, 2010. DOI: 10.1103/physrevc.82.024313.

[9] T. Eronen, A. Kankainen, and J. Äystö, "Ion traps in nuclear physics—recent results and achievements", *Progress in Particle and Nuclear Physics*, vol. 91, pp. 259–293, 2016. DOI: 10.1016/j.ppnp.2016.08.001.

[10] S. Rainville *et al.*, "A direct test of e=mc2", *Nature*, vol. 438, no. 7071, pp. 1096–1097, 2005. DOI: 10.1038/4381096a.

[11] T. Eronen *et al.*, "JYFLTRAP: A penning trap for precision mass spectroscopy and isobaric purification", *The European Physical Journal A*, vol. 48, no. 4, 2012. DOI: 10.1140/epja/i2012-12046-1.

[12] I. Moore *et al.*, "Towards commissioning the new IGISOL-4 facility", *Nuclear Instruments and Methods in Physics Research Section B: Beam Interactions with Materials and Atoms*, vol. 317, pp. 208–213, 2013. DOI: 10.1016/j.nimb.2013.06.036.

[13] W. R. Plaß, T. Dickel, and C. Scheidenberger, "Multiple-reflection time-of-flight mass spectrometry", *International Journal of Mass Spectrometry*, vol. 349-350, pp. 134–144, 2013. DOI: 10.1016/j.ijms.2013.06.005.

[14] J. Ärje *et al.*, "Submillisecond on-line mass separation of nonvolatile radioactive elements: An application of charge exchange and thermalization processes of primary recoil ions in helium", *Physical Review Letters*, vol. 54, no. 2, pp. 99–101, 1985. DOI: 10.1103/physrevlett.54.99.

[15] J. Äystö *et al.*, Eds., *Three decades of research using IGISOL technique at the University of Jyväskylä*. Springer Netherlands, 2014. DOI: 10.1007/978-94-007-5555-0.

[16] A. Nieminen *et al.*, "Beam cooler for low-energy radioactive ions", *Nuclear Instruments and Methods in Physics Research Section A: Accelerators, Spectrometers, Detectors and Associated Equipment*, vol. 469, no. 2, pp. 244–253, 2001. DOI: 10.1016/s0168-9002(00)00750-6.

[17] G. Savard *et al.*, "A new cooling technique for heavy ions in a penning trap", *Physics Letters A*, vol. 158, no. 5, pp. 247–252, 1991. DOI: 10.1016/0375-9601(91)91008-2.

[18] A. Bey *et al.*, "Beta-decay branching ratios of 62ga", *The European Physical Journal A*, vol. 36, no. 2, pp. 121–126, 2008. DOI: 10.1140/epja/i2008-10578-5.

[19] M. König *et al.*, "Quadrupole excitation of stored ion motion at the true cyclotron frequency", *International Journal of Mass Spectrometry and Ion Processes*, vol. 142, no. 1-2, pp. 95–116, 1995. DOI: 10.1016/0168-1176(95)04146-c.

[20] D. A. Nesterenko *et al.*, "Phase-imaging ion-cyclotron-resonance technique at the JYFLTRAP double penning trap mass spectrometer", *The European Physical Journal A*, vol. 54, no. 9, 2018. DOI: 10.1140/epja/i2018-12589-y.

[21] R. N. Wolf *et al.*, "Static-mirror ion capture and time focusing for electrostatic ion-beam traps and multi-reflection time-of-flight mass analyzers by use of an in-trap potential lift", *International Journal of Mass Spectrometry*, vol. 313, pp. 8–14, 2012. DOI: 10.1016/j.ijms.2011.12.006.

[22] F. Wienholtz *et al.*, "Mass-selective ion ejection from multi-reflection time-of-flight devices via a pulsed in-trap lift", *International Journal of Mass Spectrometry*, vol. 421, pp. 285–293, 2017. DOI: 10.1016/j.ijms.2017.07.016.

[23] D. A. Dahl, "Simion for the personal computer in reflection", *International Journal of Mass Spectrometry*, vol. 200, no. 1-3, pp. 3–25, 2000. DOI: 10.1016/s1387-3806(00)00305-5.

[24] F. Wienholtz *et al.*, "Improved stability of multi-reflection time-of-flight mass spectrometers through passive and active voltage stabilization", *Nuclear Instruments and Methods in Physics Research Section B: Beam Interactions with Materials and Atoms*, 2019. DOI: 10.1016/j.nimb.2019.04.061.

[25] N. E. Bradbury and R. A. Nielsen, "Absolute values of the electron mobility in hydrogen", *Physical Review*, vol. 49, no. 5, pp. 388–393, 1936. DOI: 10.1103/physrev.49.388.

[26] A. Takkinen, "Characterization of magnetof ion detector and Bradbury-Nielsen ion gate", Master's thesis, University of Jyväskylä, 2018. [Online]. Available: http://urn.fi/URN:NBN:fi:jyu-201806063022.

[27] D. Stresau *et al.*, "A new class of robust sub-nanosecond tof detectors with high dynamic range.", ETP, Sydney, Australia. Presented at the 54th ASMS Conference on Mass Spectroscopy, Seattle, Washington, Tech. Rep., 2006. [Online]. Available: https://www.etp-ms.com/file-repository/26 (visited on 12/03/2019).

[28] *Model mcs6a, 64 bit 5/(6) input 100 ps multistop tdc, multiscaler, time-of-fligh*, Fast ComTec, Oberhaching, Germany. [Online]. Available: https://www.fastcomtec.com/fwww/datashee/photon/mcs6.pdf (visited on 12/03/2019).

[29] *Mpa-nt multiparameter system software*, Fast ComTeC, Oberhaching Germany. [Online]. Available: https://www.fastcomtec.com/fwww/datashee/mpa/mpant.pdf (visited on 12/03/2019).

[30] D. Allan, "Time and frequency (time-domain) characterization, estimation, and prediction of precision clocks and oscillators", *IEEE Transactions on Ultrasonics, Ferroelectrics, and Frequency Control (ISSN 0885-3010)*, vol. UFFC-34, pp. 647–654, 1987.

[31] P. Schury *et al.*, "Wide-band mass measurements with a multi-reflection time-of-flight mass spectrograph", *International Journal of Mass Spectrometry*, vol. 359, pp. 19–25, 2014. DOI: 10.1016/j.ijms.2013.11.005.

[32] S. Purushothaman *et al.*, "Hyper-emg: A new probability distribution function composed of exponentially modified gaussian distributions to analyze asymmetric peak shapes in high-resolution time-of-flight mass spectrometry", *International Journal of Mass Spectrometry*, vol. 421, pp. 245 –254, 2017, ISSN: 1387-3806. DOI: https://doi.org/10.1016/j.ijms.2017.07.014. [Online]. Available: http://www.sciencedirect.com/science/article/pii/S1387380616302913.

[33] R. Wolf *et al.*, "ISOLTRAPs multi-reflection time-of-flight mass separator/ spectrometer", *International Journal of Mass Spectrometry*, vol. 349-350, pp. 123–133, 2013. DOI: 10.1016/j.ijms.2013.03.020.

[34] S. Lechner *et al.*, "Fluorescence detection as a new diagnostics tool for electrostatic ion beam traps", *Hyperfine Interactions*, vol. 240, no. 1, 2019. DOI: 10.1007/s10751-019-1628-1.